This is an *Accepted Manuscript*, which has been through the Royal Society of Chemistry peer review process and has been accepted for publication.

Accepted Manuscripts are published online shortly after acceptance, before technical editing, formatting and proof reading. Using this free service, authors can make their results available to the community, in citable form, before we publish the edited article. We will replace this *Accepted Manuscript* with the edited and formatted *Advance Article* as soon as it is available.

You can find more information about *Accepted Manuscripts* in the **Information for Authors**.

Please note that technical editing may introduce minor changes to the text and/or graphics, which may alter content. The journal's standard **Terms & Conditions** and the **Ethical guidelines** still apply. In no event shall the Royal Society of Chemistry be held responsible for any errors or omissions in this *Accepted Manuscript* or any consequences arising from the use of any information it contains.

Journal Name

COMMUNICATION

Novel topotactically transformed carbon-CoO-NiO-NiCo$_2$O$_4$ nanosheets hybrid hetero-structured arrays as ultrahigh performance supercapacitors

Hai Wang, Junling Guo, Chen Qing, Daming Sun, Bixiao Wang and Yiwen Tang*

A novel carbon-CoO-NiO-NiCo$_2$O$_4$ integrated electrode has been designed by reducing the hetero-structured NiCo$_2$O$_4$ nanosheets array with C$_2$H$_2$ on the nickel foam at a low temperature of 350 ℃. The topototactical transformation from NiCo$_2$O$_4$ to the integrated electrode has been first convinced and investigated. Such unique nanoarchitetures exhibit excellent electrochemical performance with ultrahigh capacitance and desirable cycle life at high rates.

To meet the increasing demand in electric energy storage for electric vehicles and mobile electronics, supercapacitors have been widely investigated and received extensive attention for their faster charge-discharge capability, longer lifespan and better safety. In general, supercapacitors are divided into two types based on different energy storage mechanisms respectively: electrical double-layer capacitors (EDLCs) and pseudocapacitors. Through electrostatic accumulation of charges in the electric double-layer near electrode/electrolyte interfaces, EDLCs express high power supply but low specific capacitance and low energy density.[1] Pseudocapacitors, electrode materials such as NiO, Co$_3$O$_4$, MnO$_2$,[2-4] possess multiple oxidation states/structures that enable rich redox reactions on the surface of electrode, which receive high specific capacitance but poor conductivity and cycling performance.

Recently, ternary NiCo$_2$O$_4$ has evoked tremendous interest for its better electrical conductivity and higher redox activity compared to nickel oxides and cobalt oxides.[5] For further promotion of the electrochemical behaviors of NiCo$_2$O$_4$, we develop a facile hydrothermal reaction and followed low temperature chemical vapor deposition (CVD) reaction to design and fabricate novel carbon-CoO-NiO on porous hierarchical NiCo$_2$O$_4$ nanosheets hetero-structured arrays (denoted as NiCo$_2$O$_4$/C NSHAs) on nickel foam. The reduction of the surface of NiCo$_2$O$_4$ was first convinced by X-ray diffraction (XRD) and selected area electron diffraction (SAED), X-ray photoelectron spectrum (XPS) and the reaction mechanism is studied. Meanwhile, there is no report on the changes of electrochemical behaviors of carbon integrated on NiCo$_2$O$_4$ so far. The construction involves the following advantages: (i) both the NiCo$_2$O$_4$ and carbon are electrochemical active materials and complementary. The porous hierarchical NiCo$_2$O$_4$ nanosheets hetero-structured arrays (NiCo$_2$O$_4$ NSHAs) provide large surface area for the carbon; simultaneously, the crystalline and disordered carbon increases the electric conductivity of NiCo$_2$O$_4$ and leads to a more hydrophilic surface respectively. Hence the redox reactions in the electrolyte are dramatically promoted. (ii) Carbon introduced and other obtained products during the CVD stage change the morphology into nanosheets with larger nanoparticles and pores, which benefits the accumulation of charges near electrode / electrolyte interfaces and shorten the diffusion length for electrons in a single particle. (iii) The CVD reaction temperature is as low as 350 ℃, which is the same as the annealing temperature of synthesizing NiCo$_2$O$_4$ from NiCo$_x$(OH)$_y$ NSHAs, suggesting the method is cost-effective and practical. As a consequence of above functions, the optimal NiCo$_2$O$_4$/C NSHAs exhibit large areal capacitance of 5.23 F cm^{-2} (2602.0 F g^{-1}) in 6 M KOH aqueous electrolyte, good rate capability and excellent cycling performance even with a rising trend after 7000 cycles.
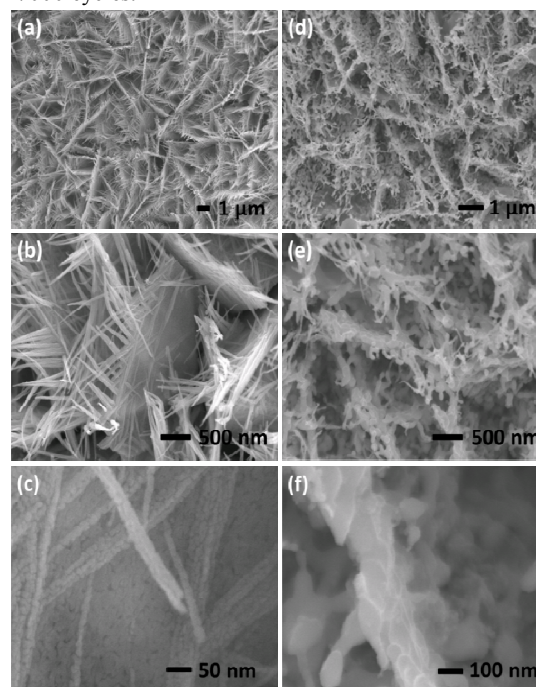
Fig. 1 (a, b, c) Low, middle, high magnification of SEM images of NiCo$_2$O$_4$ NSHAs. (d, e, f) Low, middle, high magnification of SEM images of NiCo$_2$O$_4$/C NSHAs.

The detailed synthesis procedure can be found in the ESI†. Fig. S1† shows the XRD patterns of NiCo$_2$O$_4$ and NiCo$_2$O$_4$/C NSHAs on nickel foam. The ultrahigh two peaks around 45° and 53° come from the substrate Ni. For the NiCo$_2$O$_4$ NSHAs, it is in good agreement with the spinel NiCo$_2$O$_4$ phase (JCPDS 73−1702) of (311), (400), (511), (440) planes. As to NiCo$_2$O$_4$/C NSHAs, the intensity of peaks for (511) and (440) planes is weak, and a peak around 62.5° is observed, corresponding to the (220) plane of cubic CoO (JCPDS Card No. 48-1719). The result will be discussed shortly.

Fig. 1a, b, c display the top-view field scanning electron microscopy (FESEM) images of NiCo$_2$O$_4$ NSHAs. Obviously, the hetero-structured nanosheet is composed of porous nanowall with nano-particles and nanowires grew on the nickel foam uniformly and vertically. The size distribution of the nanoparticles was about 10~20 nm. Such structure is usually observed in the transition metal oxides synthesized through annealing the pre-preparation of hydroxide and carbonate,[6-7] which gives no an exhaustive promotion for the electrochemical behaviors. Fig. 1d, e, f show the morphology after the C$_2$H$_2$ was introduced. Clearly, the overall structure kept uniform. Interestingly, the particles of nanowalls became larger. Compact nanowall changed into loose and pores between the particles became larger. Such structural transformation provides a larger surface area for the electrolyte penetration into the inner region of the electrode and permits easy access for the redox reactions.[8]
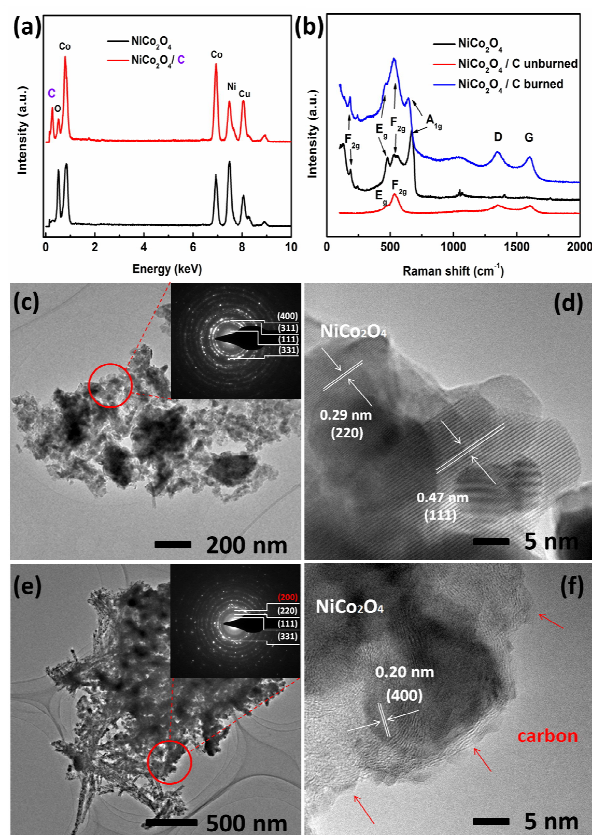

Fig. 2 (a) EDX results of NiCo$_2$O$_4$, NiCo$_2$O$_4$/C NSHAs. (b, c) Low, high resolution TEM images and SAED pattern of the NiCo$_2$O$_4$ NSHAs. (d) Raman spectrum of NiCo$_2$O$_4$, NiCo$_2$O$_4$/C NSHAs in a laser power 0.2 mW, and NiCo$_2$O$_4$/C NSHAs with partial carbon burned in a laser power 20 mW. (e, f) Low, high-resolution TEM images and SAED pattern of the NiCo$_2$O$_4$/C NSHAs.

The Energy Dispersive X-ray Spectrum (EDX) results in Fig. 2a demonstrate the carbon existed in the NiCo$_2$O$_4$/C NSHAs electrode after the C$_2$H$_2$ was introduced. The proportion of carbon in composition was tested as 5 wt. % in EDS patterns. Raman spectroscopy was used to investigate the property of carbon as shown in Fig. 2b. Peaks of black curve in 186.7, 467.8, 527.5, 644.0 cm^{-1}, are corresponding to the characteristic peaks for F$_{2g}$, E$_g$, F$_{2g}$, A$_{1g}$[9a] stretching modes of spinel NiCo$_2$O$_4$ on the nickel foam in a laser power 0.2 mW. The red curve is the untreated spectrum of NiCo$_2$O$_4$/C. The characteristic peaks of NiCo$_2$O$_4$ only left two modes E$_g$ and F$_{2g}$ around 500 cm^{-1} and other peaks disappeared. To reduce the interference, we increased the laser power from 0.2 mW to 20 mW to burn off partial carbon. The blue curve is corresponding to the burned sample. It can be seen that all the characteristic peaks of NiCo$_2$O$_4$ reveal again, which suggest that the carbon wrapping enhances the stretching behaviours of E$_g$ and F$_{2g}$ but weakens the A$_{1g}$. Such results are probably due to carbon introduced changes the exposed crystallographic directions.[9b] The tiny shift of wavenumber to lower is because of higher laser power used.[9c] D band in 1349.7 cm^{-1} and G band in 1603.1 cm^{-1} suggest the existence of carbon.[9d] Such results indicate that NiCo$_2$O$_4$/C was successfully synthesized. The higher intensity of D than G band indicates the presence of disordered carbon and structural defects, which is because of the low temperature in the synthetic process compared to others.[10-11] However, such structural defects made it easier to form hydrophilic oxygen functional groups[12] so that more efficient surface utilization in the aqueous electrolyte were received, which improve the electrochemical performance as supercapacitors.[13-14] Transmission electron microscope (TEM) was employed to get more detailed information about the carbon and the change during the CVD stage. In the typical TEM image (Fig. 2c) of NiCo$_2$O$_4$ NSHAs, the nanosheet is formed by nanoparticles as seen in the SEM image (Fig. 2c). High-resolution TEM (HRTEM) image in Fig. 2c reveals the nanoparticles have a distinct set of visible lattice fringes with internal spacings of 0.47 nm and 0.29 nm, correspond well to the (111) and (220) plane of spinel NiCo$_2$O$_4$. The corresponding SAED pattern (the inset in Fig. 2c) indicates the polycrystalline nature of the NiCo$_2$O$_4$ NSHAs, and the diffraction rings can be readily indexed to the (111), (311), (400) and (331) planes of spinel NiCo$_2$O$_4$. Fig. 2e displays the typical TEM image of NiCo$_2$O$_4$/C NSHAs, the nanoparticles of nanosheet became larger than NiCo$_2$O$_4$ as observed in the Fig. 2f. In terms of the HRTEM image in Fig. 2f, a set of lattice fringes with spacing of 0.2 nm corresponding to (400) plane of spinel NiCo$_2$O$_4$ are observed. On the surface of NiCo$_2$O$_4$, well crystalline lattice fringes with internal spacing of 0.4 nm is correspondence to the carbon with thickness in the range of 2~20 nm, which improves the electrical conductivity of NiCo$_2$O$_4$. Meanwhile, SAED pattern for Fig. 2f was also carried out (the inset in Fig. 2e). The diffraction rings are indexed to (111), (220), (331) planes of spinel NiCo$_2$O$_4$ and another ring in red excluded. The internal spacings are calculated as 0.213 nm, corresponding to the (200) plane of cubic CoO, which is in good agreement with the XRD result of NiCo$_2$O$_4$/C NSHAs. In addition, XPS was further implemented as shown in Fig. S2† and discussed in detail in the ESI†, which convinced the formation of CoO and NiO. In consequence, we can conclude that the reaction process during the CVD stage is as described below: First, the obtained hydrothermal synthesized Ni-Co hydroxide precursor, NiCo$_x$(OH)$_y$, was annealed and completely converted into spinel NiCo$_2$O$_4$ NSHAs, as soon as the reducing gas C$_2$H$_2$ was introduced,[15] the surface of the spinel NiCo$_2$O$_4$ was reduced to cubic CoO, NiO and C were formed as observed in the XRD and HRTEM results. Considering the Ni ions occupy the same position as Co ions in the oxygen octahedron of spinel structure and similar activity of both ions, the Ni ions possess the same reaction

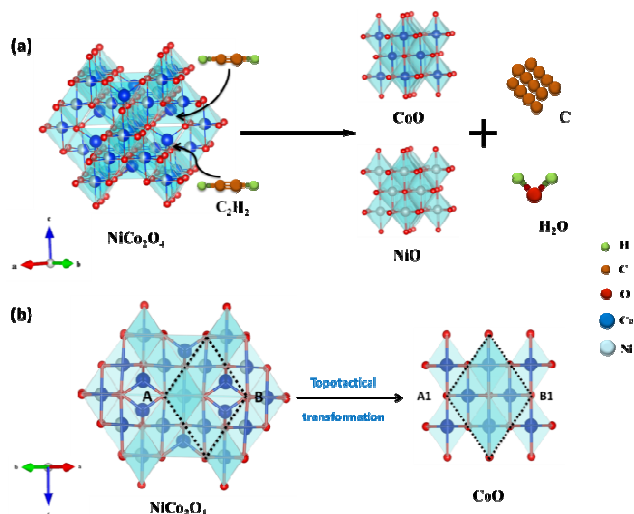process.[16-17] Thus the reaction equation is concluded as following equation:

$$NiCo_2O_4 + C_2H_2 \rightarrow NiO + 2CoO + C + H_2O$$

Fig. 3 (a) Growth mechanism of NiCo$_2$O$_4$/C NSHAs from NiCo$_2$O$_4$ NSHAs. (b) Structural illustrations viewed along [110] direction from spinel NiCo$_2$O$_4$ to cubic CoO.

The amount of NiO was half of the obtained CoO and it may be too little to observe. For the amount of carbon integrated as well as the CoO and NiO were relatively little (no obvious mass change of the active material as the C$_2$H$_2$ was introduced), the NiCo$_2$O$_4$ dominates the pseudocapacitive behavior of NiCo$_2$O$_4$/C NSHAs. We further proposed the growth mechanism of NiCo$_2$O$_4$/C NSHAs from NiCo$_2$O$_4$ NSHAs as depicted in Fig. 3a. For the spinel NiCo$_2$O$_4$ of space group Fd-3m, Co atoms and Ni atoms randomly form [CoO$_6$] as Co(III) cations and [NiO$_6$] octahedron as Ni(III) cations, while the Co(II) cations and Ni(II) cations are located in the tetrahedral sites. The products CoO(II) and NiO(II) are all cubic structure and present in the octahedral sites. Thus the transformation process from spinel to cubic structure is related to the structural relationships between the tetrahedral and octahedral oxygen anions upon a reductive change from trivalent to divalent cations.[15] We take CoO as an example to describe the transformation as the C$_2$H$_2$ was introduced. As for CoO, it can be speculated that two neighboring [CoO$_3$] tetrahedral combine into one [CoO$_6$] octahedron through a minimum ion rearrangement, as shown in the rhombic framework defined by dotted lines of Fig. 3b. Meanwhile, the crystallographic parameters of AB and A1B1 also support such assumption. The length AB of face-centered cubic (fcc) NiCo$_2$O$_4$ is calculated as 5.737 Å (at a$_o$(NiCo$_2$O$_4$)=8.114 Å) and the distance A1B1 of fcc CoO is 6.026 Å (at a$_o$(CoO)=4.261 Å). The spacing matching ratio of AB and A1B1 reaches as high as 95.2%, which further convinces the speculated reductive topotactical transformation. As a consequence, the topotactical transformation leads to the change of construction of NiCo$_2$O$_4$ into nanosheets with larger particles and pores.

The electrochemical performance of NiCo$_2$O$_4$ and NiCo$_2$O$_4$/C NSHAs on 2 × 0.5 cm^2 (active mass ~ 2 mg) nickel foams were investigated in 6 M KOH aqueous electrolyte in a three-electrode configuration. For both NiCo$_2$O$_4$ and NiCo$_2$O$_4$/C NSHAs, two oxidation peaks P1 and P2 and reduction peaks P3 and P4 are noticed in Fig. 4a, corresponding to the reversible reactions of Co^{2+}/Co^{3+} and Ni^{2+}/Ni^{3+}.[18] At a same current density of 2 mA cm^{-2}, NiCo$_2$O$_4$ and NiCo$_2$O$_4$/C can be charged to the potential 0.48V and the discharge time is 581.7s and 1278.4 s. Fig. 4c displays the

galvanostatic charge/discharge tests at various current densities from 2 mA cm^{-2} to 50 mA cm^{-2} for NiCo$_2$O$_4$ and NiCo$_2$O$_4$/C NSHAs. The discharge curves are illustrated in Fig. S3† NiCo$_2$O$_4$ NSHAs, the specific capacitance degradation is calculated to be from 2.06 F cm^{-2}
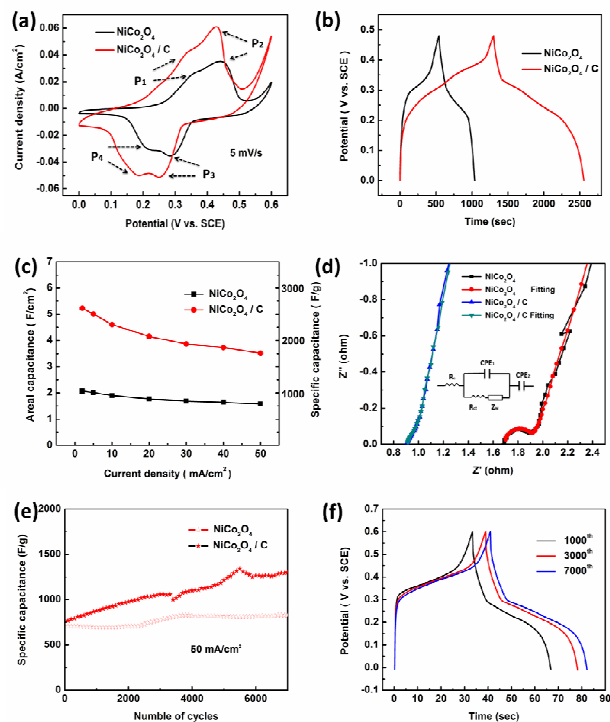

Fig. 4 Electrochemical performance of NiCo$_2$O$_4$ and NiCo$_2$O$_4$/C NSHAs: (a) CV curves at the scanning rate of 5 mV s^{-1} in the potential window 0~0.6 V; (b) Charge-discharge curves at the current density of 2 mA cm^{-2}; (c) Specific capacitance versus various current densities; (d) High frequency EIS spectrum and corresponding curve fitting; (e) Cycling performance at the current density of 50 mA cm^{-2}. (f) Charge-discharge curves of NiCo$_2$O$_4$/C NSHAs at the current density of 50 mA cm^{-2} in the 1000th, 3000th, 7000th.

to 1.57 F cm^{-2} with 76.1% retention. Good rate capability signifies NiCo$_2$O$_4$ NSHAs were good pseudocapacitors and nanostructured template. After the crystal transformation and carbon integrated, the obtained NiCo$_2$O$_4$/C NSHAs expressed an ultrahigh area capacitance 5.23 F cm^{-2} (2602.0 F g^{-1}), which is the highest capacitance received for NiCo$_2$O$_4$ and higher than NiCo$_2$O$_4$ nanowires 743 F g^{-1} at 1 A g^{-1},[7] NiCo$_2$O$_4$ nanoneedles, 3.12 F cm^{-2} at 1.11 mA cm^{-2},[19] NiCo$_2$O$_4$@MnO$_2$ 3.31 F cm^{-2} at 2 mA cm^{-2},[20] 2.244 F cm^{-2} at 2 mA cm^{-2},[21] NiCo$_2$O$_4$@ NiCo$_2$O$_4$ nanosheets 1.55 F cm^{-2} at 2 mA cm^{-2},[22] NiCo$_2$O$_4$@ NiCo$_2$O$_4$ microrods 678 F g^{-1} at 6 A g^{-1},[23] And also higher than those carbon materials integrated, NiCo$_2$O$_4$/RGO composites, 835 F g^{-1} at 1 A g^{-1},[24] NiCo$_2$O$_4$ nanowires/graphene, 737 F g^{-1} at 1 A g^{-1}.[25] Such outstanding performance was further investigated by Electrochemical Impedance Spectroscopy (EIS) spectrum. The corresponding Nyquist plots and fitting results (inset circuit is the equivalent circuit) of NiCo$_2$O$_4$ and NiCo$_2$O$_4$/C NSHAs are shown in Fig. 4d, which illustrate the solution resistance R$_s$, charge-transfer R$_{ct}$ and Warburg resistance Z$_w$.[26] Impressively, the solution resistance dramatically reduces from 1.69 Ω to 0.88 Ω at the same test condition, indicating that the surface of the NiCo$_2$O$_4$/C NSHAs electrode were highly hydrophilic due to the hydrophilic oxygen functional groups on the surface, which also conforms to the Raman results. Meanwhile, the absence of complete semicircle region for R$_{ct}$ indicates low faradaic resistance of the hybrid arrays and good electrical conductivity between arrays and the nickel

foams.[27] In the low frequency part of EIS spectrum as shown in Fig. S4†, , the Z_w of $NiCo_2O_4$/C NSHAs became higher, leading to a relatively low rate retention compared to $NiCo_2O_4$ NSHAs, which was probably caused by products with more phases generated. By a long-term cycling test at a high current density of 50 mA cm^{-2}, the excellent cycling performance is illustrated in Fig. 4e. After 7000 cycles, there even exists a rising tendency. Such outstanding cycling performance can be ascribed to the hetero-architecture and multiple phases[22, 28]: (i) The hetero-structure arrays, which support and connect with each other, help to alleviate the structure damage caused by volume expansion during the cycling process, resulting in an enhanced stability and cycle performance. (ii) Multiple phases lead to longer activation time, which gives a rising tendency of cycling performance for $NiCo_2O_4$/C NSHAs. The trend is further convinced by the chosen 1th, 3000th, 7000th charge-discharge curves in Fig. 4f. Nearly 100 % Coulombic efficiency and stable charge-discharge platform suggest that such $NiCo_2O_4$/C NSHAs hybrid electrode a promising energy-storage material.

Conclusions

In conclusion, a facile and practical strategy has been developed to construct $NiCo_2O_4$/C NSHAs with high electrochemical performance for supercapacitors. We also investigate the reaction mechanism for growth of carbon and the reduction process of $NiCo_2O_4$ during the CVD stage and such method could be applied to cobaltates. The as-fabricated $NiCo_2O_4$/C NSHAs electrode delivers the highest specific capacitance of 5.23 F cm^{-2} (2602.0 F g^{-1}) and excellent cycling performance, which confirms the ultrathin carbon layer for the promotion of high-performance advanced integrated array electrode.
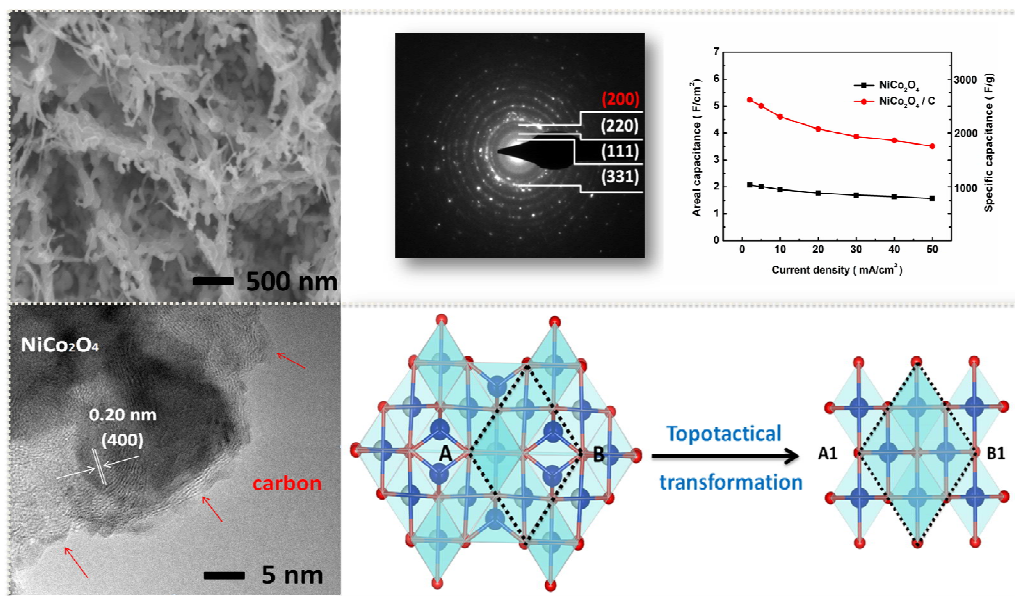
Acknowledgment

Notes and references

*Institute of Nanoscience and Nanotechnology, Department of Physics, Central China Normal University, Wuhan, 430079, China. Fax: 86 27 67867947; Tel.: 86 27 67867947; E-mail: ywtang@phy.ccnu.edu.cn**

1 (a) J. R. Miller, P. Simon, *Science*, 2008, **321**, 651; (b) P. Simon and Y. Gogotsi, *Nat. Mater.*, 2008, **7**, 845.
2 J. H. Kim, S. H. Kang, J. Y. Kim, N. R. Neale and A. J. Frank, *Chem. Commun.*, 2011, **47**, 5214.
3 C. Z. Yuan, L. Yang, L. R. Hou, L. F. Shen, X. G. Zhang and X. W. Lou, *Energy Environ. Sci.*, 2012, **5**, 7883.
4 Z. P. Sun, S. Firdoz, E. Y. Yap, L. Li and X. M. Lu, *Nanoscale*, 2013, **5**, 4379.
5 G. Q. Zhang, X. W. Lou, *Adv. Mater.*, 2012, **25 (7)**, 976.
6 C. Guan, X. L. Li, Z. L. Wang, X. H. Cao, C. Soci, H. Zhang and H. J. Fan, *Adv. Mater.*, 2012, **24**, 4186.
7 H. Jiang, J. Ma and C. Z. Li, *Chem. Commun.*, 2012,**48**, 4465.
8 H. L. Wang and H. J. Dai, *Chem. Soc. Rev.*, 2013, **42**, 3088-3113.
9 (a) L. Huang, D. C. Chen, Y. Ding, S. Feng, Z. L. Wang and M. L. Liu, *Nano Lett.*, 2013, **13**, 3135. (b) M. N. Iliev, P. Silwal, B. Loukya, R. Datta, D. H. Kim, N. D. Todorov, N. Pachauri, and A. Gupta, *J. Appl. Phys.*, 2013, **114**, 033514. (c) C. F. Windisch Jr, G. J. Exarhos, S. K. Sjarma, *J. Appl. Phys.*, 2002, **92(9)**, 5572. (d)A.N. Obraztsov, A.V. Tyurnina, E.A. Obraztsova, A.A. Zolotukhin, B. Liu, K.C. Chin, A.T.S. Wee, Carbon, 2008, **46**, 963.
10 D. Mattia, M. P. Rossi, B. M. Kim, G. Korneva, H. H. Bau and Y. Gogotso, *J. Phys. Chem. B*, 2006, **110**, 9850.
11 T. Xiao, B. J. Heng, X. Y. Hu and Y. W. Tang, J. Phys. Chem. C, 2011, **115**, 25155.
12 J. Jiang, J. P. Liu, W. W. Zhou, J. H. Zhu, X. T. Huang, X. Y. Qi, H. Zhang and T. Yu, *Energy Environ. Sci.*, 2011, **4**, 5000.
13 H. Zhang, G. P. Cao and Y. S. Yang, *Energy Environ. Sci.*, 2009, **2**, 932.
14 D. Y. Qu, *J. Power Sources,* 2002, **109**, 403.
15 S. L. Xiong, J. S. Chen, X. W. Lou and H. C. Zeng, *Adv. Funct. Mater.*, 2012, **22**, 861.
16 X. Y. Liu. Y. Q. Zhang, X. H. Xia, S. J. Shi, X. L. Wang, C. D. Gu, J. P. Tu, *J. Power Sources*, 2013, **239**, 157.
17 J. F. Marco, J. R. Gancedo, M. Gracia, J. L. Gautier, E. I. Rios, H. M. Palmer, C. Greaves and F. J. Berry, *J. Mater. Chem.*, 2013, **1**, 3171.
18 X. Wang, X.D. Han, M.F. Lim, N.D. Singh, C.L. Gan, M. Jan, P.S. Lee, *J. Phys. Chem. C*, 2012, **116**, 12448.
19 G. Q. Zhang, H. B. Wu, H. E. Hoster, M. C. Park and X. W. Lou, *Energy Environ. Sci.,* 2012, **5**, 9453.
20 L. Yu, G. Q. Zhang, C. Z. Yuan and X. W. Lou, *Chem. Commun.,* 2013, **49**, 137.
21 K. B. Xu, W. Y. Li, Q. Liu, B. Li, X. J. Liu, L. An, X. Z. G. Chen, R. J. Zou and J. Q. Hu, *J. Mater. Chem. A*, 2014, **2**, 4795.
22 X. Y. Liu, S. J. Shi, Q. Q. Xiong, L. Li, Y. J. Zhang, H. Tang, C. D. Gu, X. L. Wang and J. P. Tu, *ACS Appl. Mater. Interfaces,* 2013, **5 (17)**, 8790.
23 X. F. Lu, D. J. Wu, R. Z. Li, Q. Li, S. H. Ye, Y. X. Tong and G. R. Li, *J. Mater. Chem. A,* 2014, **2**, 4706.
24 H. W. Wang, Z. A. Hu, Y. Q. Chang, Y. L. Chen, H. Y. Wu, Z. Y. Zhang and Y. Y. Yang, *J. Mater. Chem.*, 2011, **21**, 10504.
25 G. Y. He, L. Wang, H. Q. Chen, X. Q. Sun, X. Wang, *Mater. Lett.,* 2013, **98**, 164.
26 C. Zhou, Y. W. Zhang, Y. Y. Li and J. P. Liu, *Nano Lett.*, 2013, **13 (5)**, 2078.
27 Q. Wu, Y. X. Xu, Z. Y. Yao, A. R. Liu and G. Q. Shi, *ACS Nano*, 2010, **4 (4)**, 1963.
28 X.Y. Liu, Y.Q. Zhang, X.H. Xia, S.J. Shi, Y. Lu, X.L. Wang, C.D. Gu, J.P. Tu, *J. Power Sources* 2013, **239**, 157.

ChemComm Accepted Manuscript

Graphical Abstract

A novel carbon-CoO-NiO-NiCo$_2$O$_4$ integrated electrode has been designed by reducing the hetero-structured NiCo$_2$O$_4$ nanosheets array with C$_2$H$_2$ on the nickel foam at a low temperature of 350℃. The topototactical transformation from NiCo$_2$O$_4$ to the integrated electrode has been first convinced and investigated. Such unique nanoarchitetures exhibit excellent electrochemical performance with ultrahigh capacitance and desirable cycle life at high rates.